Biocompatible and stable ZnO quantum dots generated by functionalization with siloxane-core PAMAM dendrons

Ralph-Oliver Moussodia, Lavinia Balan, Christophe Merlin, Christian Mustin, Raphaël Schneider

Biocompatible and stable ZnO quantum dots generated by functionalization with siloxane-core PAMAM dendrons

Ralph-Olivier Moussodia,[a] Lavinia Balan,[b] Christophe Merlin,[c] Christian Mustin,[d] and Raphaël Schneider*[a]

Received (in XXX, XXX) Xth XXXXXXXXX 200X, Accepted Xth XXXXXXXXX 200X
First published on the web Xth XXXXXXXXX 200X
DOI: 10.1039/b000000x

Despite the growing interest of quantum dots (QDs) in biological applications, there are many concerns regarding the potential accumulation and toxic effects of Cd-containg QDs in animals and humans. Zinc oxide QDs are promising alternatives for diagnosis and imaging but their aqueous instability has markedly limited their use. Generations 1, 2 and 3 (noted G1, G2, and G3, respectively) of new poly(amidoamine) (PAMAM) dendrons bearing a siloxane group at the focal point were prepared from 3-aminopropyltrimethoxysilane. Using tetramethylammonium hydroxide as cross-linking agent, hydrophobic oleate-capped ZnO QDs were functionalized with G1 or G2 dendrons, as evidenced by FT-IR, UV-visible and XPS analyses, and were successfully transferred in aqueous solution. AFM and TEM images show that ZnO@G1 and ZnO@G2 QDs have a spherical shape with average crystalline sizes of 5.3 and 5.1 nm, respectively. Immediately after dispersion in water, ZnO@G1 and ZnO@G2 QDs exhibit a broad and strong visible emission peak centered at 550 nm with a quantum yield of ca. 18%. A strong increase of photoluminescence quantum yields was observed over time and values up to 59% could be reached after ca. 20 days of storage in water at room temperature. The good quantum yields and the stabilities of PAMAM-dendron capped ZnO QDs ensured their potential applications in cell imaging. ZnO@G2 were successfully used for the labelling of the Gram + bacterium *Staphylococcus aureus*. The biocompatibility of these QDs is markedly improved compared to Cd-based ones as growth inhibition tests showed that ZnO@G2 QDs could be used with concentrations up to 1 mM without altering the cell growth of the *Escherichia coli* bacterium while most Cd-containing QDs exhibit cytotoxicity already at the nM level.

.

Introduction

Colloidal semiconductor nanocrystals, called quantum dots (QDs), are nanometer-scale luminescent inorganic materials that have found numerous applications in bio-imaging and bio-detection.[1] Owing to the effect of quantum confinement, QDs show exceptional physical and chemical properties such as sharp and symmetrical emission spectra, high quantum yield (QY), good photo- and chemical stability, and size-dependent emission-wavelength tunability.[2] Recent findings have highlighted the acute toxicity of II-VI semiconductor QDs without an external layer of a nontoxic material on biological systems and shed a doubt on the future applicability of these nanocrystals, particularly in view of recent environmental regulations.[3] This toxicity results mainly from the decomposition and release of heavy metal ions and formation of reactive oxygen species.[4] Synthesis of low toxicity QDs and especially Cd-free QDs is the most challenging aspect of working with these materials in biological and medical fields. A promising member of the Cd-free QD family is ZnO.

ZnO is a direct band gap (3.37 eV) semiconductor with a relatively high exciton binding energy (60 meV) which has found various applications in optical, electronic and sensing devices.[5] However, contrary to II-VI semiconductors such as CdSe and CdTe, ZnO QDs have received very little attention as biological labelling agents. Indeed, conventional ZnO QDs are not stable in water because water molecules are able to attack the luminescent centers on the surface and destroy them rapidly.[6] In recent years, methods of preparing luminescent ZnO QDs in an aqueous phase have been improved. A series of ZnO nanocrystals embedded in hydrophilic polymers have been synthesized[7] but these materials show only modest fluorescence QY or are too large to be used in biological applications. Indeed, with large-sized probes, diffusion and circulation processes are significantly reduced resulting in increased nonspecific binding.[8] Retaining the small probe size is critical for successful *in vivo* applications and to date, only three routes have been reported for the synthesis of nanometer-sized water-soluble ZnO QDs. Jana *et al.* described ZnO QDs capped with 3-aminopropyltrimethoxysilane where the amine groups at the periphery contribute to the stability of these QDs.[6] Very recently, Xiong *et al.* reported the preparation of stable ZnO@polymer core-shell nanoparticles with an average diameter of ca. 3-4 nm and the first example of the use of these QDs in cell imaging.[9] We have recently demonstrated the use of poly(ethylene glycol) (PEG) siloxane for the transfer of hydrophobic ZnO QDs in water with preservation of their luminescent properties.[10] However, PEG surface ligands did not offer surface groups that can be conjugated with bioactive

molecules. This limitation reduced the materials' flexibility in bio-related applications. Due to their branched nature, the presence of multivalent surface groups available for attachment of surface moities, and high water affinity, poly(amidoamine) (PAMAM) dendrimers offer significant potential as versatile carriers for enhancing bioavailability of drugs and nanoparticles.[11] Here, we report a facile strategy to synthesize highly luminescent water-soluble ZnO QDs by covalent attachment of PAMAM dendrons bearing a reactive siloxane group at the focal point. Luminescent ZnO QDs were successfully used for the imaging of the Gram + bacteria *Staphylococcus aureus*. Cytotoxicity experiments showed that these QDs could be used with concentrations up to 1 mM without altering cell growth.

Experimental

A. Materials

All reagents were purchased from Aldrich at the highest available purity, and used without further purification. Millipore water was used in all experiments.

B. Measurements

Routine nuclear magnetic resonance were recorded on a Brucker AM200 spectrometer operating at 200 MHz. Chemical shifts are reported in ppm, relative to the solvent peak, and are given downfield from tetramethylsilane (TMS). Splitting pattern abbreviations are as follows: s = singlet, d = doublet, dd = double doublet, t = triplet, td = triplet of doublets, m = multiplet. Electrospray ionization (ESI) mass spectra were recorded on a Surveyor mass spectrometer. Moisture-sensitive reactions were carried out under a dry nitrogen atmosphere in flame-dried glassware. Solvents were distilled before use under nitrogen. Absorption spectra were recorded on a Perkin-Elmer (Lambda 2, Courtaboeuf, France) UV-visible spectrophotometer. Fluorescence spectra were recorded on a Fluorolog-3 spectrofluorimeter F222 (Jobin Yvon, Longjumeau, France) equipped with a thermostated cell compartment (25°C), using a 450 W Xenon lamp. The QY values were determined by the following equation according to the method described by Crosby *et al.*[12] QY (sample) = $(F_{sample}/F_{ref})(A_{ref}/A_{sample})(n_{sample}^2/n_{ref}^2)QY_{(ref)}$, where F, A and n are the measured fluorescence (area under the emission peak), the absorbance at the excitation wavelength, and the refractive index of the solvent, respectively. Rhodamine 6G in ethanol was chosen as a reference standard (QY = 95%).[13] FT-IR spectra were recorded on a Vector 22 spectrometer using 2 mg of QDs and 198 mg of KBr to prepare pellets. To determine the morphology and the diameters of the nanoparticles, the samples were analyzed *ex situ* by Atomic Force Microscopy (AFM) and by Transmission Electron Microscopy (TEM). AFM characterization was carried out using a Digital Instruments Nanoscope III. AFM measurements were done by taping mode using a Si_3N_4 tip with resonance frequency and spring constant being 100 kHz and 0.6 $N.m^{-1}$, respectively to provide surface topography. TEM images were taken by placing a drop of the particles in water onto a carbon film supported copper grid. Samples were studied using a Philips CM20 instrument with LaB_6 cathode operating at 200 kV. XPS measurements were performed at a residual pressure of 10^{-9} mbar, using a KRATOS Axis Ultra electron energy analyzer operating with an Al Kα monochromatic source. Fluorescence images were acquired using a laser scanning head (Radiance 2100 Rainbow, Biorad) coupled with an inverted microscope (Nikon TU 2000) equipped with a 60x objective (Apo VC Nikon, NA = 1.4).

C. Synthesis

Synthesis of oleate-capped ZnO QDs. Zinc acetate (220 mg, 1.2 mmol) was dissolved in ethanol (20 mL) at a temperature below 50°C under vigorous stirring. Oleic acid (70 µL, 0.22 mmol) was then added and the mixture was heated to reflux. In a separate flask, tetramethylammonium hydroxide (360 mg, 1.99 mmol) was dissolved in refluxing ethanol (5 mL). This solution was then rapidly injected in the flask containing $Zn(OAc)_2$ and oleic acid and the mixture was refluxed for 2 min. The mixture was then diluted with EtOH (50 mL) and cooled down to 0°C with an ice-bath. A white precipitate of ZnO nanoparticles appeared. Particles were centrifugated (15 min at 4000 rpm) with removal of the supernatant. The resulting oleate-capped ZnO QDs were washed several times with ethanol, in which they are insoluble, and finally suspended in toluene (10 mL). Oleate-capped ZnO QDs were stored at 4°C in the dark.

Synthesis of ZnO@G1 QDs. Under a nitrogen atmosphere, the oleate-capped ZnO QDs previously prepared were dispersed in 10 mL toluene and treated with 1 mL of a 0.1 M solution of G1 dendron in EtOH. After 5 min stirring at room temperature, 1 mL of a 0.3 M solution of tetramethylammonium hydroxide (TMAH) in EtOH was injected and the temperature was set at 85°C. After 45 min, the solution was allowed to cool and nanoparticles isolated by centrifugation (4000 rpm, 15 min). After removal of the supernatant, ZnO@G1 QDs were washed three times with toluene in which they are insoluble. QDs were then redispersed in water and were further purified by successive precipitation-solubilization rounds using acetone as bad-solvent. After drying for 5 h *in vacuo*, QDs were redispersed in water for further experiments.

Synthesis of ZnO@G2 QDs. ZnO@G2 nanoparticles were prepared analogously to the reaction above, with the exception that 1 mL of a 0.6 M TMAH solution in EtOH was added to the oleate-capped ZnO QDs and to the G2 dendron.

Cytotoxicity tests. Bacteria were routinely cultured at 30°C in Luria broth Miller [Difco] (1% Tryptone, 0.5% Yeast Extract, 1% NaCl). For growth experiments, bacteria were pregrown in shaking conical flasks filled to 20% of their volume with LB medium without QD until the cultures reached mid log phase. At OD_{595} around 0.2, cultures were

diluted one-tenth in prewarmed LB medium supplemented with the desired concentration of QD and the optical density was measured at intervals. All growth experiments were carried out in the dark to limit both cell damage by light-excited QDs and photo-oxidation reactions at QDs' surfaces.

Results and discussion

First-, second- and third-generation (respectively G1, G2 and G3) PAMAM dendrons were prepared by divergent synthesis through repetitive Michael addition using methyl acrylate and amidation with ethylene diamine starting from 3-aminopropyltrimethoxysilane (Scheme 1 and ESI†) using the method previously described.[14] Among the solvents used for the amidation step, the best results were obtained in methanol. Alkoxy group exchange (up to 30%) was observed in ethanol. Temperature also had an influence on the reaction yield. Proper amidation without alteration of the trimethoxysilane moiety and formation of large quantities of by-products could only be achieved by stirring the half-generation ester-terminated dendrons (G0.5, G1.5 and G2.5) with an excess of ethylene diamine in methanol at 5°C for 120 h. Under these optimized conditions, G1, G2, and G3 dendrons were isolated in quantitative yields and their structures confirmed by HRMS, and ^{1}H and ^{13}C NMR studies.

Hydrophobic oleate-capped ZnO QDs were prepared by the sol-gel method[6,15,16] by basic hydrolysis of $Zn(OAc)_2$ with a few modifications. $Zn(OAc)_2$ is first dissolved at a temperature below 50°C in anhydrous EtOH and oleic acid is then added. An EtOH solution of TMAH is then injected, the solution refluxed for 2 min and then directly diluted with EtOH and cooled to 0°C. The white powder obtained was collected by centrifugation, washed 2 times with ethanol and dried *in vacuo* at room temperature. TEM images showed that oleate-capped ZnO QDs possess an average diameter of 5.1 nm (data not shown). These nanocrystals could be resuspended in chloroform or toluene, indicating the presence of the long-chain carboxylate ligand shell. The solutions thus obtained were found to show bright green-yellow luminescence under UV excitation (QY = 24% in toluene), thereby indicating the formation of ZnO QDs.

Oleate is a relatively weak stabilizer ionically bound to the surface of ZnO colloids, while siloxanes have a strong affinity with hydroxylated surfaces and form strong covalent Si-O bonds with them.[17] The $Zn(OH)_2$ shell coating the ZnO surface was used for the modification of ZnO nanoparticles.[18] The covalent anchorage of G1 dendron at the surface of oleate-capped ZnO QDs was first investigated using TMAH as cross-linking reagent in an EtOH/toluene mixture at 80°C. Amounts of TMAH were modified from those previously optimized for the reaction of PEG-siloxanes with ZnO QDs.[10] Initial studies focused upon the reaction of G1 dendron with ZnO QDs. Poor transfers (less than 10%) of the hydrophobic ZnO nanoparticles were obtained using less than 2 eq TMAH relative to the siloxane, with no evidence for self-nucleation of the siloxane. For the G2 dendron, the ligand exchanges were complete using 6 eq TMAH. These results reflect the acidic character of the hydrogen atoms of the PAMAM amide

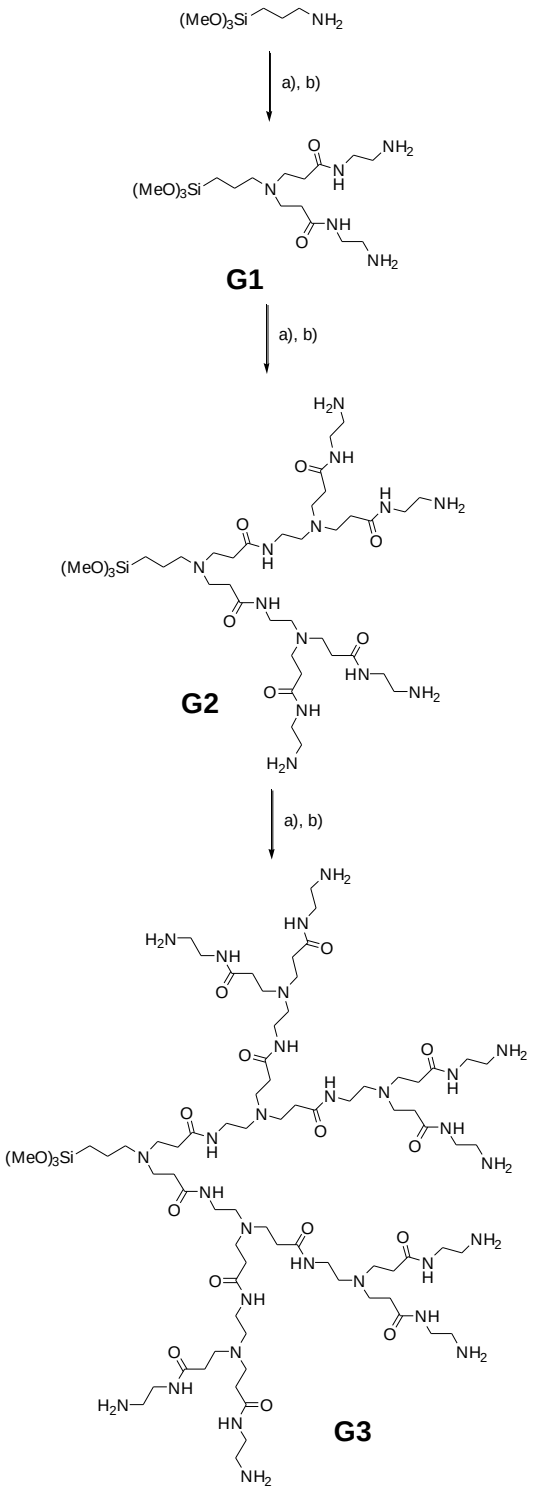

Scheme 1 Synthesis of siloxane-core PAMAM dendrons; reaction conditions: (a) methyl acrylate, MeOH, rt, 48 h; (b) ethylene diamine, MeOH, 5°C, 120 h.

bonds (pKa = 17.0) which partially consume the TMAH base used for the hydrolysis of the siloxane moiety. Under these optimized conditions, G1 and G2 were successfully attached on ZnO QDs surface hydroxyl groups. After cooling to room temperature, the crude QDs were recovered by centrifugation,

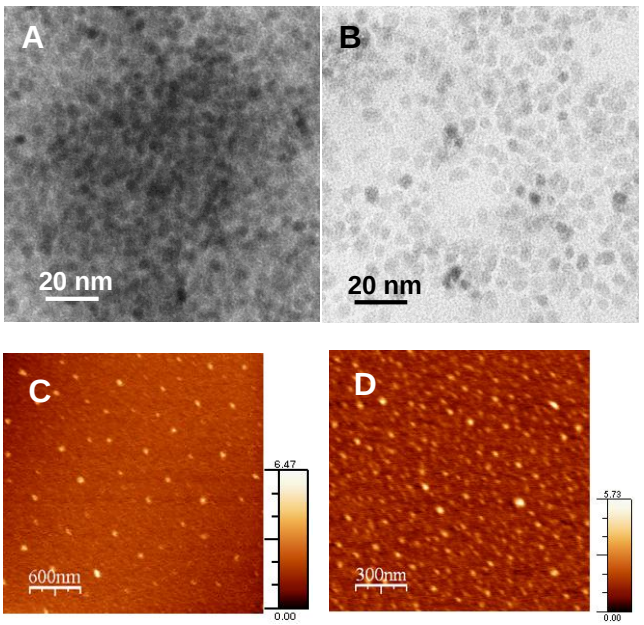

Fig. 1 Bright field TEM and AFM images of (A) and (C) ZnO@G1, and (B) and (D) ZnO@G2 QDs.

redispersed in water and purified by successive precipitation-solubilization rounds using acetone as bad-solvent. The pellets were highly soluble in water, less soluble in methanol and ethanol, and insoluble in e.g. chloroform, toluene and less polar solvents. The QDs obtained after functionalization with G1 and G2 dendrons, designated as ZnO@G1 and ZnO@G2 respectively, were redispersed in water or phosphate-buffer saline (PBS) for further experiments. The absorption spectra of the nanocrystals did not change upon the surface replacement of the original oleate ligands by the siloxane-based dendron ligands (see Fig. S1 in ESI†). Compared to the band-edge of bulk ZnO, the excitonic peak bandgap absorption of the nanoparticles is located at much higher energies (3.59 eV) due to the quantum confinement effect. The relatively pronounced absorption peaks show that the size distributions of ZnO QDs are nearly monodispersed after surface functionalization with G1 or G2 dendrons. Compared to oleate-capped ZnO QDs, there are two additional peaks in the 250-300 nm region. These peaks are assigned as typical $\pi \rightarrow \pi^*$ and $n \rightarrow \pi^*$ transitions of the PAMAM carbonyl groups and appeared at 260 and 283 nm, respectively. For both QDs, the absorption edge value of 3.59 eV afforded ZnO cluster diameters of 5.0 nm as predicted by the Brus' effective mass model.[19] This value agrees well with diameters obtained by Transmission Electron Microscopy (TEM) and Atomic Force Microscopy (AFM) (analysis of ca. 100 nanocrystals in each TEM image yielded average crystal diameters of 5.3 ± 0.5 and 5.1 ± 0.6 nm for ZnO@G1 and ZnO@G2 QDs, respectively) (Fig. 1 and Figs. S2 and S3 in the ESI†). In both samples, the ZnO QDs appeared to be spherical, uniform, and disperse. Since oleate-capped ZnO QDs had an average diameter of 5.1 nm, no variation of QDs diameters was noticed after their surface modification with G1 or G2 dendrons.

Confirmation of particles surface modification was attained *via* X-ray photoelectron spectroscopy (XPS) (Fig. 2 and Fig. S4 in the ESI†) and FT-IR (Fig. 3). The XPS scan survey spectrum of the samples show only the peaks of Zn, O, Si, N, and C elements and no peaks of any other elements were observed. As seen on Fig. 2a, the peak of Zn 2p3/2 appears at 1021.0 eV, confirming that the Zn element exists only in the form of Zn^{2+} linked to an oxygen atom. Fig. 2b shows that the O 1s peak is somewhat asymmetric, suggesting that there are at least three kinds of oxygen species on the sample surface. The deconvoluted peaks at ca. 530.0, 531.3 and 533.3 eV can respectively be attributed to the lattice oxygens of ZnO, to the oxygens of the surface hydroxyl groups and to the oxygen atoms of the amide groups. The Si 2p element is characterized by a single peak located at a binding energy of 101.4 eV (Fig. 2c). Finally, the N 1s signal (Fig. 2d) shows two components at 399.3 and 402.0 eV corresponding respectively to the primary and secondary nitrogen atoms and to the amide nitrogens. The N/Zn and Si/Zn ratios obtained from the XPS analyses were used to estimate the number of dendrons anchored at the surface of ZnO@G1 and ZnO@G2 QDs. Using a hexagonal wurtzite crystal structure for ZnO[20] with lattices parameters of a = 0.325 nm and c = 0.520 nm,[21] ZnO@G1 and ZnO@G2 dendrons were respectively found to be covered by *ca*. 2800 G1 and 900 G2 dendrons. FT-IR spectra of purified and dried powders before and after surface functionalization with G1 or G2 dendrons are given in Fig. 3. The strong vibration band at ca. 465 cm^{-1} observed in all spectra is attributed to the stretching mode of ZnO.[22] The two peaks at 1409 and 1575 cm^{-1} in Fig. 3a are respectively attributed to the symmetric and asymmetric stretching vibrations of the oleate

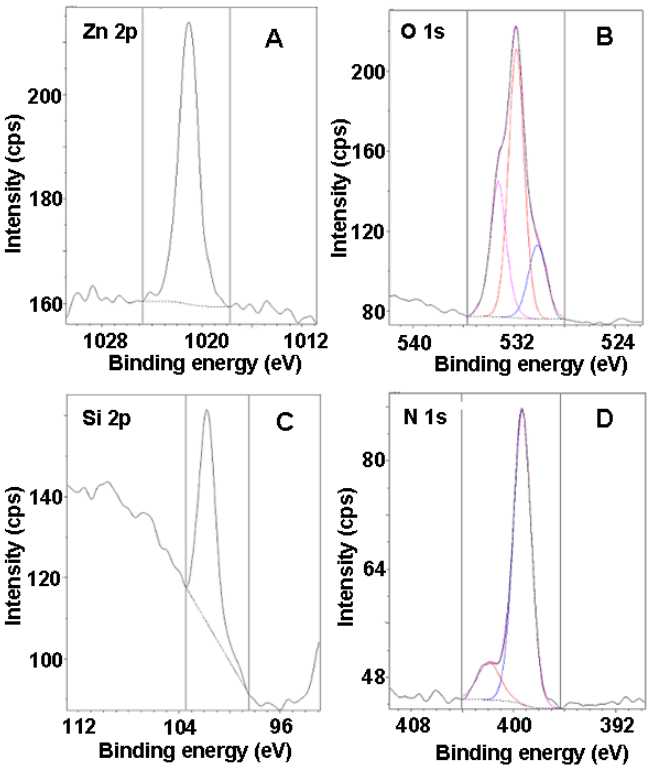

Fig. 2 XPS spectra of the ZnO@G1 quantum dots. The Zn 2p, O 1s, Si 2p, and N 1s emissions are presented.

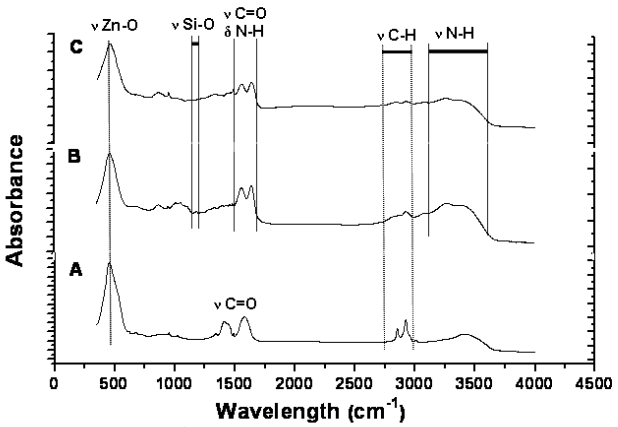

Fig. 3 FT-IR spectra of (A) ZnO/oleate QDs, (B) ZnO@G1 QDs, and (C) ZnO@G2 QDs.

carboxylate group and vanish upon functionalization with G1 and G2 dendrons (Fig. 3b and c).[23] In spectra 3b and 3c, the weaks peaks at respectively 1188 and 1160 cm^{-1} are characteristic of the Si-O-Si symmetrical stretching vibrations.[24] These spectra also displayed the bands assigned to amides, N-H asymmetric stretching (3260-3271 cm^{-1}), C=O stretching (1640-1647 cm^{-1}), N-H bending (1540-1548 cm^{-1}) and of the terminal primary amines (N-H stretching at 3384 cm^{-1}).[25]

ZnO@G1 and ZnO@G2 nanocrystals show a broad visible luminescence centered at *ca* 550 nm and a relatively weak UV emission band at *ca* 416 nm attributed to exciton recombination (Fig. 4). The green emission at 550 nm, commonly referred to as a deep-level or trap-state emission,[26] is related to a singly ionized oxygen vacancy in ZnO and results from radiative recombination of a photogenerated hole with an electron occupying the oxygen vacancy.[27] The QYs of ZnO@G1 and ZnO@G2 QDs, measured immediately after dispersion in water and determined by using rhodamine 6G in ethanol as reference, were found to be 19 and 17%, respectively.

Considerable differences were noticed after attempting the cross-linking of the G3 dendron at the surface of oleate-capped ZnO QDs. No aggregation of QDs was noticed after reaction with G3 dendron in the presence of TMAH (up to 14 eq were used for the anchorage of the G3 dendron) and a clear nanoparticle solution was obtained after transfer in water. The average diameter of QDs obtained after reaction was found to be close to that of the starting oleate-capped ZnO QDs (5.1 nm). Whereas absorption characteristics of nanoparticles was practically unchanged, the photoluminescence (PL) color changed from yellow to blue and the PL peak position was observed at ca. 425 nm ligands (see Fig. S5 in the ESI†). A similar phenomenon was observed when oleate-capped ZnO QDs were treated with the G2 PAMAM dendrimer possessing no siloxane function at the focal point (Fig. 5). On the basis of our current data and previous literature results,[28] it is reasonable to suggest that the ZnO-G3 dendrimer nanocomposite is formed by dendrimer molecules adsorbing on the ZnO nanoparticles. In addition, FT-IR measurements showed that the absorption band of the amino terminal groups of the G3 dendrimer was slightly shifted to a higher value (NH stretching at 3402 cm^{-1}) whereas this shift was not observed with ZnO@G1 and ZnO@G2 QDs. We assume that

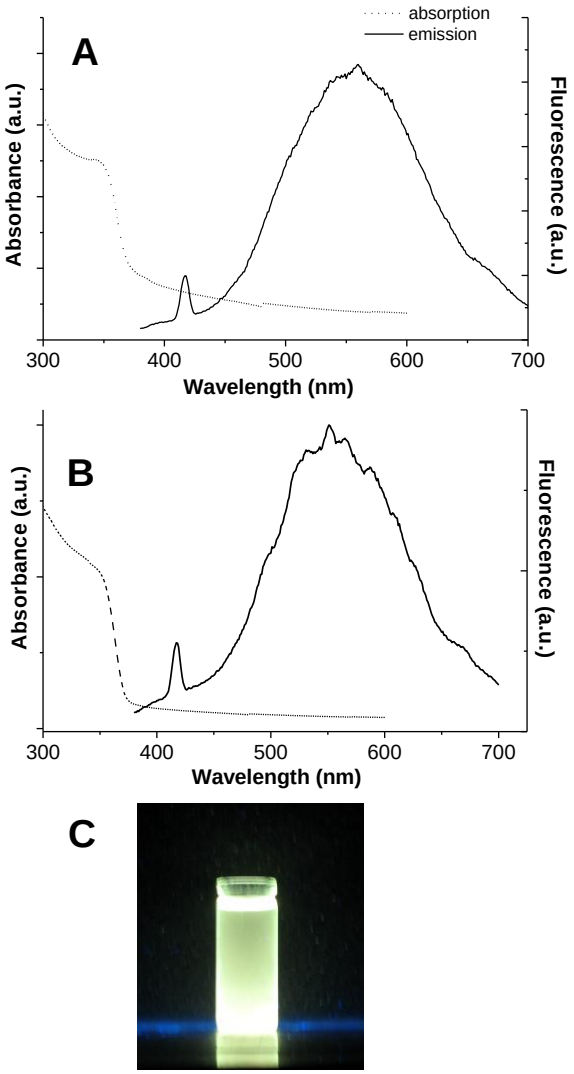

Fig. 4 Room temperature absorption and photoluminescence spectra recorded after excitation at 365 nm of (A) ZnO@G1 and (B) ZnO@G2 QDs. (C) Photography of ZnO@G2 QDs dispersed in water and illuminated with an ultraviolet lamp.

the bulky and flexible structure of the G3 PAMAM ramification and especially the strongly coordinating 8 primary amine terminal groups strongly interact with electron deficient particles surface sites thus disrupting the anchorage of the siloxane moiety at the surface of ZnO QDs and altering PL.

The stability of ZnO@G1 and ZnO@G2 QDs was studied by dispersing the nanoparticles in water and monitoring the change in PL intensity after excitation at 350 nm as a function of time using rhodamine 6G as reference (Fig. 6). Data obtained clearly indicated a strong increase of PL intensity at the beginning of the experiment. Almost stable PL was obtained *ca.* 15 days after dispersion. The enhancement of the 550 nm emission is respectively of 3.1 and 2.5 fold for ZnO@G1 and ZnO@G2 QDs after 20 days storage in water and a PL QYs of ca. 59 and 43% were attained for ZnO@G1 and ZnO@G2 nanocrystals,

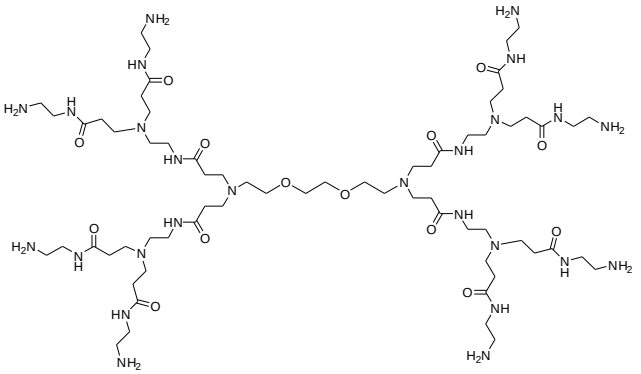

Fig. 5 Chemical structure of the G2 dendrimer bearing no siloxane unit at the focal point.

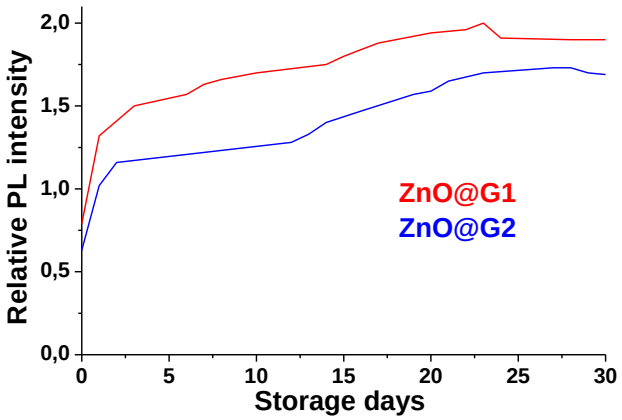

Fig. 6 Changes in photoluminescence intensity of dendrons capped ZnO QDs as a function of time

respectively. These PL QYs values compare favorably with those recently reported by Xiang *et al*. for ZnO QDs embedded in PEG-methacrylate polymers (20-50%).[9] In the meantime, no noticeable change in the absorption and emission spectra of ZnO QDs was observed during the storage time. Compared to the results obtained with PEG-*bis*-carboxymethyl-coated ZnO nanoparticles,[29] it is unlikely that the PL enhancement observed originates from the coordination of the nitrogen or oxygen atoms of the PAMAM ramification with the ZnO particles surface. Indeed, this interaction should result in a decrease of surface defects and thus to an increase of the ZnO excitonic emission. We privilege a surface ordering of the siloxane-capped ZnO QDs which protects the surface of the QDs from water attack at the luminescent centers. Nevertheless, the present findings may provide an effective method for improving the PL properties of ZnO nanocrystals.

The usefulness of PAMAM dendrons capped-ZnO QDs, in the context of bio-imaging probe design, was demonstrated in a labelling experiment with *S. aureus*. Before labelling, *S. aureus* bacterial cells only displayed a minimal autofluorescence signal (data not shown). After 1 hour incubation at room temperature with a 1 µM ZnO@G2 QDs suspension, the bacterial cells clearly appeared fluorescently labelled indicating a QD accumulation (Fig. 7a and Fig. S6 in the ESI†). The mean surfaces (0.5 ± 0.16 µm^2) and the circularity (0.92 ± 0.06) of fluorescent objects determined by

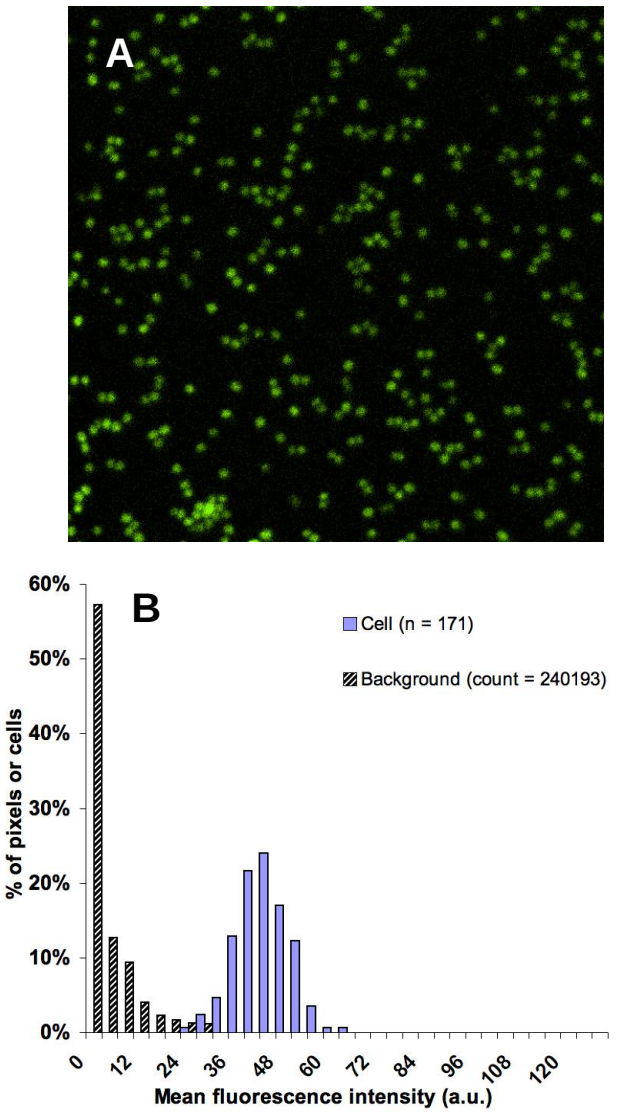

Fig. 7 (a) Confocal microscopy image of *S. aureus* cells labelled with ZnO@G2 QDs (green fluorescence, 530-560 nm). Image width and heigth are equal to 44.6 µm (pixel size 87 nm) and analysed depth = 0.3 µm. (b) Histogram for the population of cells from the micrograph.

laser scanning microscopy show individual cell labelling without aggregation of the imaged biological material. As shown by Fig. 7b, the variability of labelling intensity can be determined from the analysis of a large number of individual cell fluorescence. The ZnO@G2 QDs labelling of *S. aureus* cells vary per individual (shown as a histogram) and was found to have a bell-shaped distribution (mean = 45.2 ± 6.6) which may result from physiological variability. Upon incubation, positively charged ZnO@G2 QDs may self-assemble on the negatively charged bacterial surfaces of the *S. aureus* cells. Throughout the observation time (ca. 1 h), only negligible fluorescence fading was observed, thus showing the photostability of the ZnO QDs under prolonged and repeated imaging conditions. Similar experiments carried out with an other bacterial species, e.g. the Gram - *E. coli*, showed

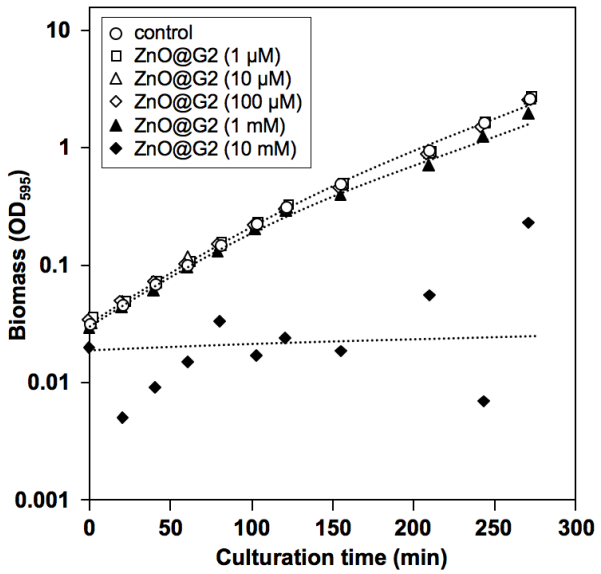

Fig. 8 Growth inhibition of *E. coli* MG1655 by ZnO@G2 QDs. MG1655 was cultivated in LB medium until OD_{595} reached 0.2 and was then diluted in LB medium supplemented with various concentrations of ZnO@G2 QDs.

only weak cell-QD association. Interestingly, other labelling experiments with different cells and ZnO QDs showed the same tendency between Gram + and Gram – (data not shown). At present, we suppose that positively charged QDs may accumulate on cells through electrostatic interactions with teichoic and lipoteichoic acids present on the surface of this Gram + bacterium while the outer membrane of the Gram -, composed of lipopolysaccharides, would be less receptive to QDs.

Recently, we developed a test to evaluate the toxicity of QDs toward bacteria.[30] With this respect, it was shown that CdTe-core QDs were already toxic against *E. coli* cells at nanomolar concentration as seen by a decrease of growth rate. The toxixity test was repeated with the ZnO@G2 QDs in the same experimental conditions. Contrary to CdTe QDs, ZnO@G2 QDs displayed a remarquably weak toxicity as no growth alteration was detected until 1 mM (Fig. 8). Growth alteration became visible at 10 mM. The antibacterial effect of ZnO@G2 QDs was found to be 10^6 times less pronounced than thioglycolic acid-capped CdTe QDs further highlighting the promising potential of these nanoparticles for *in vivo* bioimaging.[30,31]

Conclusions

In summary, we have demonstrated that stable and water-soluble ZnO QDs can be prepared through surface functionalization of these nanocrystals with siloxane-core PAMAM dendrons G1 and G2. Those dendron-coated nanocrystals are structurally simple and the corresponding ligand monolayer is very thin in comparison to other stabilizing approaches. The potential of ZnO@G2 QDs as fluorescent probes was demonstrated by the labelling of *S. aureus* bacteria cells. The surface amine groups of the PAMAM ligands should facilitate further surface functionalization with targeting ligands, opening up the way to direct ZnO nanoparticles toward specific biological material. Because of their weak toxicity, these QDs should play an important role in a variety of nanocrystal-based biomedical applications in a near future. We are currently investigating the possibility of tuning the emission wavelengths of ZnO QDs by doping for *in vivo* biological labelling.

Acknowledgements

The authors thank Dr. Fabienne Quilès (LCPME, Nancy-University) for FT-IR spectra, Olivier Soppera (UMR CNRS 7525, Mulhouse) for AFM images and Jacques Lambert (LCPME, Nancy-University) for acquiring the XPS spectra.

Notes and references

[a] *DCPR, Nancy-University, CNRS, 1 rue Grandville, BP 20451, 54001 Nancy, France. Fax: +33 3 83 37 81 20; Tel: +33 3 83 17 50 53; E-mail: raphael.schneider@ensic.inpl-nancy.fr*
[b] *DPG, Université de Haute Alsace, UMR 7525, 3 rue Alfred Werner, 68093 Mulhouse, France.*
[c] *LCPME, Nancy-University, CNRS, 405 rue de Vandoeuvre, 54600 Villers-lès-Nancy, France.*
[d] *LIMOS, Nancy-University, CNRS, Faculté des Sciences, 54506 Vandoeuvre-lès-Nancy, France.*

† Electronic Supplementary Information (ESI) available: Synthesis and analytical data of G1, G2 and G3 dendrons, experimental procedures, full TEM images and particles size distributions, XPS spectra of ZnO@G2 QDs, absorption and emission spectra of ZnO@G3 QDs, AFM image of ZnO@G3 QDs, and confocal imaging experiments. See DOI: 10.1039/b000000x/

1 (a) J. K. Jaiswal, H. Mattoussi, J. M. Mauro and S. M. Simon, *Nat. Biotechnol.*, 2003, **21**, 47. (b) D. R. Larson, W. R. Zipfel, R. M. Williams, S. W. Clark, M. P. Bruchez, F. W. Wise and W. W. Webb, *Science*, 2003, **300**, 1434. (c) X. Michalet, F. F. Pinaud, L. A. Bentolila, J. M. Tsay, S. Doose, J. J. Li, G. Sundaresan, A. M. Wu, S. S. Gambhir and S. Weiss, *Science*, 2005, **307**, 538.

2 (a) C. B. Murray, C. R. Kagan and M. G. Bawendi, *Annu. Rev. Mater. Sci*., 2000, **30**, 545. (b) M. Bruchez, Jr., M. Moronne, P. Gin, S. Weiss and A. P. Alivisatos, *Science*, 1998, **281**, 2013. (c) W. C. W. Chan and S. Nie, *Science*, 1998, **281**, 2016.

3 (a) E. Chang, N. Thekkek, W. W. Yu, V. L. Colvin and R. Drezek, *Small*, 2006, **2**, 1412. (b) N. Lewinski, V. Colvin and R. Drezek, *Small*, 2008, **4**, 26. (c) S. J. Klaine, P. J. J. Alvarez, G. E. Batley, T. F. Fernandes, R. D. Handy, D. Y. Lyon, S. Mahendra, M. J. McLaughlin and J. R. Lead, *Environ. Toxicol. Chem*., 2008, **27**, 1825. (d) Y. Su, Y. He, H. Lu, L. Sai, Q. Li, W. Li, L. Wang, P. Shen, Q. Huang and C. Fan, *Biomaterials*, 2009, **30**, 19.

4 (a) C. Kirchner, T. Liedl, S. Kudera, T. Pellegrino, A. M. Javier, H. E. Gaub, S. Stollzle, N. Fertig and W. J. Parak, *Nano Lett*., 2005, **5**, 331. (b) Y. Zhang, J. He, P. N. Wang, J. Y. Chen, Z. J. Lu, D. R. Lu, J. Guo, C. C. Wang and W. L. Yang, *J. Am. Chem. Soc*., 2006, **128**, 13396. (c) J. Ma, J. –Y. Chen, Y. Zhang, P. –N. Wang, J. Guo, W. –L. Yang and C. –C. Wang, *J. Phys. Chem. C*, 2007, **111**, 12012. (d) Z. Lu, C. M. Li, H. Bao, Y. Qiao, Y. Toh and X. Yang, *Langmuir*, 2008, **24**, 5445.

5 For reviews, see: (a) A. B. Djurisic and Y. H. Leung, *Small*, 2006, **2**, 944. (b) C. Klingshirn, *Phys. Stat. Sol. (b)*, 2007, **244**, 3027. For recent reports, see: (c) H. –M. Xiong, Z. –D. Wang, D. –P. Liu, J. -S. Chen, Y. –G. Wang and Y. –Y. Xia, *Adv. Func. Mater*., 2005, **15**,

1751. (d) Y. Qiu and S. Yang, *Adv. Func. Mater*., 2007, **17**, 1345. (e) E. Badaeva, Y. Feng, D. R. Gamelin and X. Li, *New J. Phys*., 2008, **10**, 055013. (f) H. –H. Yu, M. K. F. Wong, E. M. Ali, J. Y. Ying, *Chem. Commun*., 2008, 4912.
6 N. R. Jana, H. Yu, E. M. Ali, Y. Zheng and J. Y. Ying, *Chem. Commun*., 2007, 1406.
7 (a) H. –M. Xiong, D. –P. Liu, Y. -Y. Xia and J. –S. Chen, *Chem. Mater*., 2005, **17**, 3062. (b) H. –M. Xiong, Z. –D. Wang, D. –P. Liu, J. –S. Chen, Y. -G. Wang and Y. –Y. Xia, *Adv. Func. Mater*., 2005, **15**, 1751.
8 X. H. Gao, L. Yang, J. A. Petros, F. F. Marshall, J. W. Simons and S. M. Niu, *Curr. Opin. Biotechnol*., 2005, **16**, 63.
9 H. –M. Xiong, Y. Xu, Q. –G. Ren and Y. –Y. Xia, *J. Am. Chem. Soc*., 2008, **130**, 7522.
10 R. –O. Moussodia, L. Balan and R. Schneider, *New J. Chem*., 2008, **32**, 1388.
11 A. D'Emanuele, D. Attwood, R. Abu-Rmaileh, *Dendrimers*, in *Encyclopedia of Pharmaceutical Technology*, Marcel Dekker, New York, 2003, pp 1-21.
12 G. A. Crosby and J. N. Demas, *J. Phys. Chem*., 1971, **75**, 991.
13 M. Fischer and J. Georges, *Chem. Phys. Lett*. 1996, **206**, 115.
14 D.A. Tomalia, B. Huang, D.R. Swanson, H.M. Brothers II and J.W. Klimash, *Tetrahedron*, 2003, **59**, 3799.
15 N. R. Jana, Y. Chen and X. Peng, *Chem. Mater*., 2004, **16**, 3931.
16 H. –H. Yu, M. K. F. Wong, E. M. Ali, J. Y. Ying, *Chem. Commun*. 2008, 4912.
17 (a) A. B. Bourlinos, A. Stassinopoulos, D. Anglos, R. Herrera, S. H. Anastasiadis, D. Petridis, E. P. Giannelis, *Small*, 2006, **2**, 513. (b) R. De Palma, S. Peeters, M. J. Van Bael, H. Van den Rul, K. Bonroy, W. Laureyn, J. Mullens, G. Borghs and G. Maes, *Chem. Mater*., 2007, **19**, 1821. (c) C. G. Allen, D. J. Baker, J. M. Albin, H. E. Oertli, D. T. Gillaspie, D. C. Olson, T. E. Furtak and R. T. Collins, *Langmuir*, 2008, **24**, 13393.
18 H. Zhou, H. Alves, D. M. Hofmann, B.K. Meyer, G. Kaczmarczyk, A. Hoffmann, C. Thomsen, *Phys. Stat. Sol*. 2002, **229**, 825.
19 L. E. Brus, *J. Phys. Chem*., 1986, **90**, 2555.
20 E. A. Meulenkamp, *J. Phys. Chem. B*, 1998, **102**, 5566.
21 H. –P. Cong, S. –H. Yu, *Adv. Func. Mater*., 2007, **17**, 1814.
22 S. Maensiri, P. Laokul and V. Promarak, *J. Crystal Growth*, 2006, **289**, 10.
23 Y. –S. Fu, X. –W. Du, S. A. Kulinich, J. –S. Qiu, W. –J. Qin, R. Li, J. Sun, and J. Liu, *J. Am. Chem. Soc*., 2007, **129**, 16029.
24 X. –Y. Shang, Z. –K. Zhu, J. Yin, and X. –D. Ma, *Chem. Mater*., 2002, **14**, 71.
25 A. Manna, T. Imae, K. Aoi, M. Okada and T. Yogo, *Chem. Mater*., 2001, **13**, 1674.
26 (a) A. B. Djuris, W. C. H. Choy, V. A. L. Roy, Y. H. Leung, C. Y. Kwong, K. W. Cheah, T. K. G. Rao, W. K. Chan, H. F. Lui and C. Surya, *Adv. Funct. Mater*. 2004, **14**, 856. (b) Q. Wan and T. H. Wang, *Appl. Phys. Lett*., 2005, **87**, 083105. (c) F. Q. He and Y. P. Zhao, *Appl. Phys. Lett*., 2006, **88**, 193113. (d) D. S. Bohle and C. J. Spina, *J. Am. Chem. Soc*., 2007, **129**, 12380.
27 K. Vanheusden, W. L. Warren, C. H. Seager, D. R. Tallant, J. A. Voigt and B. E. Gnade, *J. Appl. Phys*., 1996, **79**, 7983.
28 C. Zhang, S. O'Brien and L. Balogh, *J. Phys. Chem. B*, 2002, **106**, 10316.
29 B. K. Woo, W. Chen, A. G. Joly and R. Sammynaiken, *J. Phys. Chem. C*, 2008, **112**, 14292.
30 R. Schneider, C. Wolpert, H. Guilloteau, L. Balan, J. Lambert and C. Merlin, *Nanotechnology*, 2009, **20**, 225101.
31 Z. Lu, C. M. Li, H. Bao, Y. Qiao, Y. Toh and X. Yang *Langmuir*, 2008, **24**, 5445.

